Published in final edited form as:
Ther Deliv. 2013 February ; 4(2): 161–175. doi:10.4155/tde.12.144.

Nanomedicine for Uterine Leiomyoma Therapy

Hazem Ali[1,2], **Gokhan Kilic**[1], **Kathleen Vincent**[1,3], **Massoud Motamedi**[3], and **Erik Rytting**[1,3,4,*]

[1]Department of Obstetrics & Gynecology, University of Texas Medical Branch, Galveston, Texas 77555

[3]Center for Biomedical Engineering, University of Texas Medical Branch, Galveston, Texas 77555

[4]Department of Pharmacology & Toxicology, University of Texas Medical Branch, Galveston, Texas 77555

Abstract

Aims—The purpose of this work was to engineer polymeric nanoparticles to encapsulate and deliver 2-methoxyestradiol, a potential antitumor drug for treatment of uterine leiomyoma (fibroids), the most common hormone-dependent pathology affecting women of reproductive age.

Materials & Methods—Encapsulation efficiency and drug release from the nanoparticles were monitored by HPLC. Cell morphology and *in vitro* cytotoxicity experiments were carried out in a human leiomyoma cell line (huLM).

Results—The nanoparticles displayed high encapsulation efficiency (>86%), which was verified by differential scanning calorimetry and X-ray diffraction. Excellent long-term stability of the nanoparticles and gradual drug release without burst were also observed. Cellular uptake of fluorescent nanoparticles was confirmed by confocal imaging. The drug-loaded poly(lactic acid) and poly(lactic-co-glycolic acid) nanoparticles induced cytotoxicity in huLM cells to a significantly greater extent than the free drug at 0.35 μM.

Conclusion—This novel approach represents a potential fertility-preserving alternative to hysterectomy.

Introduction

Uterine leiomyomas, commonly known as fibroids, are benign solid tumors that are considered a major women's health problem because of symptoms of pelvic pain, heavy menstrual bleeding, very painful and prolonged menstrual periods, increased morbidity, and reproductive dysfunction [1,2]. A uterine fibroid projecting into the uterine cavity may block implantation of the embryo, or it may cause problems later in pregnancy. African American women tend to suffer from symptoms of uterine fibroids three to four times as often as white women [3,4].

Although expensive, surgical intervention via hysterectomy or myomectomy remains the primary treatment option for such tumors [5]. Such surgical management has its associated risks and also compromises fertility [6]. Moreover, the costs associated with lost time at the

*Corresponding author: Erik Rytting, University of Texas Medical Branch, 301 University Boulevard, Galveston, Texas 77555-0587, USA, Tel: +1-409-772-2777, Fax: +1-409-747-0266, erik.rytting@utmb.edu.
[2]Current address: Moores Cancer Center, University of California San Diego, La Jolla, CA 92093

Disclosure
The authors declare no competing financial interests.

patient's job and recovery times represent additional obstacles for a patient to undergo surgery. For these reasons, non-surgical treatment modalities that improve symptoms and attain fibroid shrinkage are needed.

It has been reported that leiomyomas express Bcl-2 protein [7] and mRNAs of collagen Type I and Type III [8]. Thus, apoptosis-inducing medications—such as 2-methoxyestradiol—which block the synthesis of extracellular matrix, could serve as an effective treatment option [6]. Recently, the potential use of 2-methoxyestradiol (2-ME) as an antitumor agent has gained interest for the treatment of uterine fibroids [6]. It induces cell death through inhibition of DNA synthesis, cell proliferation, collagen synthesis, cyclin D_1 and cyclin B_1 expression, and phosphorylation of retinoblastoma protein [9]. It also causes fragmentation of tubulin and up-regulation of Cdk inhibitor p27 expression [9].

However, a significant barrier to successful leiomyoma therapy with is the challenge of delivering the required therapeutic concentration to the uterine fibroids. The poor aqueous solubility of 2-ME leads to poor bioavailability [10]. Besides insufficient plasma levels, drug therapy might also fail because of widespread drug distribution to the non-target tissues, or even therapeutic resistance of the target tissues due to poor drug penetration and/or rapid drug clearance from the tissue of interest, precluding prolonged local drug presence. Therefore, it is prudent to develop a delivery system containing 2-ME that effectively and safely reduces fibroid size and ameliorates the associated symptoms.

The use of nanoparticles as carriers for successful delivery of 2-ME for potential leiomyoma therapy has not been reported thus far. Encapsulating 2-ME into nanoparticles could increase 2-ME penetrability into fibroids. The slow clearance and controlled-release properties offered by nanoparticles might improve the delivery of drug to these dense tumors.

Nanosuspensions are aqueous colloidal dispersions with particles up to 1000 nm in size, the matrix of which is composed of biodegradable and biocompatible materials [11]. The drug can be dissolved, entrapped, or attached to the nanoparticle matrix [11]. Encapsulating drugs in polymeric nanoparticles can further increase *in vivo* drug stability [12]. Various polymers have been used in drug delivery research to effectively target the drug to the tissue of interest, thereby increasing its therapeutic value and simultaneously minimizing the associated side effects [13]. Among biodegradable and biocompatible polymers, poly(DL-lactide-*co*-glycolide) (PLGA), has received much interest in the field of drug delivery [14–18] because of degradation profile [19] and prolonged drug release which can be modified based upon the molecular weight, the copolymer composition, and the structure of nanoparticles [20]. Polyanhydrides represent another class of biodegradable polymers.

Copolymerization of poly(sebacic acid) (PSA) and poly(ethylene glycol) (PEG) produces PSA-*co*-PEG, which has been shown to control the release of a variety of drug molecules [21].

We have designed and constructed novel nanoparticles loaded with 2-ME that could be used to enhance therapeutic effects of 2-ME for treatment of uterine leiomyomas. To examine the cytotoxic effects of 2-ME delivered via nanoparticles, we have performed *in vitro* studies to (1) assess the physicochemical properties of the 2-ME-loaded nanoparticles, such as particle size, surface morphology, drug encapsulation efficiency, crystallinity, *in vitro* drug release, and stability; and (2) evaluate the *in vitro* cytotoxicity of the 2-ME-loaded nanoparticles against human leiomyoma cells (huLM).

Materials & Methods

Polymer synthesis

• **Synthesis of sebacic acid prepolymer—**Synthesis was performed under the same conditions explained previously [22]. In brief, 10 g of sebacic acid (Sigma-Aldrich, MO, USA) was refluxed with 100 mL of acetic anhydride (Acros Organics, NJ, USA) under dry nitrogen for 60 minutes, cooled to room temperature and dried using a rotary evaporator for about 120 minutes. The precipitated product was then lyophilized overnight to remove solvent traces. The sebacic acid prepolymer was recrystallized from dry toluene (Acros Organics), washed with anhydrous ethyl ether (Acros Organics), and then dried by vacuum.

• **Synthesis of poly(ethylene glycol) (PEG) prepolymer—**Synthesis was performed under the same conditions explained previously [22]. Approximately 40 grams of hydroxyl-terminated PEG (MW=8000) (Spectrum Chemical Corporation, CA, USA) was dissolved in 300 mL of chloroform (Fischer Scientific, NJ, USA). Succinic anhydride (5.0 g) (Acros Organics) and 5 mL of pyridine (Acros Organics) were added, and the mixture was reacted for 72 hours at 60 °C. After cooling the solution, the product was dissolved in 1N hydrochloric acid, extracted with chloroform, and dried with anhydrous sulfate. Excess solvents were removed under vacuum. Ten grams of the product (polyoxyethylene dicarboxylic acid) were refluxed with 200 mL of acetic anhydride under dry nitrogen for 90 minutes and evaporated to dryness using a rotary evaporator. The residue was extracted with diethyl ether and dried under vacuum.

• **Synthesis of poly(sebacic acid) (PSA)—**PSA was prepared by melt polycondensation under high vacuum as described previously [22]. Briefly, 0.5 g of sebacic acid prepolymer was placed in a flask and immersed in an oil bath at 150–200°C. Monomers were allowed to melt and a strong nitrogen sweep was performed for 30 seconds every 15 minutes to agitate the molten mixture. By applying high vacuum, acetic anhydride was collected in a liquid nitrogen trap. At the end of reaction, PSA was allowed to cool and was dissolved in chloroform. The solution was added drop-wise into excess hexane. The crystallized product (PSA) was collected, filtered, and dried under vacuum.

• **Synthesis of PSA-co-PEG—**PSA-*co*-PEG copolymer (10% PEG) was prepared by melt polycondensation under high vacuum as reported previously [22]. Briefly, sebacic acid (450 g) and PEG prepolymers (50 g) were placed in a round-bottom flask with a stopcock adapter which was immersed in an oil bath at 150–200°C. Monomers were allowed to melt and a strong nitrogen sweep was performed for 30 seconds every 15 minutes to agitate the molten mixture. A high vacuum was applied to collect acetic anhydride in a liquid nitrogen trap. At the end of reaction, PSA-*co*-PEG was allowed to cool and was dissolved in chloroform. The solution was added drop-wise into excess hexane. The crystallized product (PSA-*co*-PEG) was collected, filtered, and dried under vacuum.

• **Characterization of the synthesized polymers (PSA and PSA-co-PEG)—**The synthesized polymers (PSA and PSA-*co*-PEG) were then dissolved in deuterated chloroform, and the structures of PSA and PSA-PEG were confirmed by using high resolution Proton Nuclear Magnetic Resonance (^{1}H-NMR) (Varian Inova NMR spectrometer operating at 600 MHz and 20°C). The melting endotherms of the dried polymers were also determined by thermal analysis using a Q200 differential scanning calorimeter (DSC) (TA Instruments-Waters LLC, DE, USA). Samples (2–10 mg) were placed in hermetically sealed aluminum pans and were heated from 20–150°C at a rate of 10°C/min. Melting endotherms were analyzed using Universal Analysis 2000 version 4.7A software (TA Instruments-Waters LLC, DE, USA).

Preparation of polymeric nanoparticles

Polymeric nanoparticles (Table 1) were prepared by a single emulsion/solvent evaporation method as described previously [19]. Briefly, the polymer (20 mg) and 2-ME (1.0 mg) (Sigma-Aldrich, MO, USA) were dissolved in 1.2 mL of an acetone:dichloromethane mixture (1:5 ratio) (Acros Organics). The mixture was then injected into 20 mL of aqueous phase containing 1% polyvinyl alcohol (PVA) (MP Biomedicals, OH, USA) (magnetically stirred at 500 rpm). The o/w emulsion was homogenized for 2 minutes at 40% amplitude and 90% pulsation using a Vibracell™ ultrasonic homogenizer, model VCX750 (Sonics & Materials, Inc., CT, USA). The resulting colloidal suspension was continuously stirred (850 rpm) under a fume hood for 4–5 hours to allow complete evaporation of the organic solvents.

Measurement of particle size, size distribution, and zeta potential (ζ)

Nanoparticle dispersions were diluted to 10% with double distilled water and their corresponding average particle size and polydispersity index (PDI) were measured by photon correlation spectroscopy at 25°C using a High Performance Particle Size analyzer (Malvern Instruments, UK). Zeta potential (ζ) was measured by laser Doppler velocimetry using a Zetasizer 2000 (Malvern Instruments, UK). Analyses were performed in triplicate.

Determination of nanoparticle encapsulation efficiency

Encapsulation efficiency (EE) was determined to assess the incorporation of 2-ME in the nanoparticles after preparation. It was determined by measuring the concentration of free 2-ME in the aqueous phase of the nanoparticle suspension. Approximately 500 μL of the nanoparticle dispersion were placed in the upper chamber of a Vivaspin® filter assembly (molecular weight cutoff 100 kDa). The assembly was then centrifuged at 3000 rpm for 15 minutes at 25°C using an Eppendorf 5810R centrifuge (Hamburg, Germany). The nanoparticles and encapsulated 2-ME remained in the upper chamber, but the aqueous dispersion medium containing the free unencapsulated 2-ME moved to the sample recovery chamber through the filter membrane. After separation, the amount of free 2-ME in the dispersion medium was quantified by a validated HPLC method (described below). The EE was then calculated from the following equation:

$$\text{Encapsulation efficiency} = \frac{\text{Mass of drug added} - \text{Mass of free drug in the aqueous dispersion}}{\text{Mass of drug added}} \times 100\%$$

For HPLC analysis of 2-ME, the aqueous solutions were injected into a Symmetry® C_{18} analytical column (4.6×75 mm). Isocratic elution was performed using acetonitrile:water (50:50) as a mobile phase at 1 mL/min. 2-ME was identified by a photodiode array detector at 287 nm. As indicated in the following section, the method has been validated by assessment of the system suitability, limit of detection and quantitation, linearity, precision, accuracy, specificity, auto-sampler stability, and recovery.

HPLC method validation for 2-ME

Details concerning the HPLC method and validation procedures are described in the Supplementary Data files accompanying this manuscript.

In vitro drug release

The release of 2-ME from nanoparticles was performed at 37°C under sink conditions. 500 μL of the dispersions were suspended in 500 μL of phosphate buffered saline (PBS, pH 7.4) containing 1.0% (w/v) Tween® 80 to maintain sink. Several vials were prepared and shaken

(50 rpm) in a hot box (37°C). At each time point, 500 μL of the nanoparticle dispersion were placed in the upper chamber of the filter assembly (100 kDa molecular weight cutoff, Millipore Corporation, MA, USA). The assembly was then centrifuged at 3000 rpm for 15 minutes at 25°C using Eppendorf® 5810R centrifuge (Hamburg, Germany) to separate the released 2-ME from the nanoparticles. The filtrate was diluted with the mobile phase and injected into HPLC (as described above) to determine the concentration of the released 2-ME. Experiments were carried out in triplicate, and results are expressed as mean ± standard deviation.

Cryo-electron microscopy (cryo-EM)

Cryo-EM was utilized to observe the nanoparticles' morphology. To minimize the potential morphological changes during specimen preparation and imaging, the nanoparticles were vitrified as reported previously on holey carbon film grids (C-flat™, Protochips, NC, USA) [23]. Briefly, nanoparticle dispersions were applied to the holey films in a volume of ~ 2 μl, blotted with filter paper, and plunged into liquid ethane cooled in a liquid nitrogen bath. Frozen grids were stored under liquid nitrogen and transferred to a cryo-specimen 626 holder (Gatan, Inc., CA, USA) under liquid nitrogen before loading them into a JEOL 2200 electron microscope with a field emission gun operating at 200 keV. Grids were maintained at near-liquid nitrogen temperature (−172 to −180°C) during imaging. Nanoparticles were imaged at 25,000x indicated microscope magnification with a 4k × 4k slow-scan CCD camera (UltraScan 895, Gatan, Inc., CA, USA) using a low-dose imaging procedure [23].

Freeze-drying

Prior to X-ray diffraction and differential scanning calorimetric (DSC) studies, nanoparticle dispersions were frozen at −80°C. Samples were then lyophilized for 24 hours using a Labconco bench type freeze-dryer (Labconco Corporation, MO, USA) at a temperature of −50°C and a vacuum of 0.055 mbar. The resultant lyophilized products were subjected to X-ray and DSC analysis as described below.

X-ray diffraction measurements

The crystallinity of the 2-ME-loaded nanoparticles was evaluated at room temperature by using a DIP2030 X-ray diffractometer (Yokohama, Japan). X-ray diffraction patterns were obtained by wide-angle X-ray scattering (2θ=5–30°, step size = 0.04) using a MacScience DIP2030H-VLM dual 30 cm diameter imaging plate detector which is combined with an M06XHF22, 100 μm ultra-fine-focus high-brilliancy X-ray generator and RIGAKU Blue focusing multilayer optics. Data of the scattered radiation were recorded at an anode voltage of 40 kV and a current of 30 mA. The generated data were processed through FIT2D software (provided electronically by Dr. Joseph Reibenspies, Texas A&M University, TX, USA) to convert the image into a two-dimensional plot. The x-axis represents 2θ, and the y-axis represents the intensity of diffraction.

Differential scanning calorimetry (DSC) measurements

Thermal analysis was performed to verify absence of interaction between 2-ME and the polymers and to confirm the presence of 2-ME in amorphous form (not crystalline form). DSC analyses were performed using a Q200 DSC. Samples (2–3 mg), hermetically sealed in aluminum pans, were first heated at a scan rate of 10°C/min from 20°C to 200°C and then allowed to cool to 10°C to observe the exothermic phase. During thermal scans, the crucible was purged with nitrogen. The generated data were analyzed with Universal Analysis 2000 software.

In vitro cytotoxicity studies with human leiomyoma cells (huLM)

• Cell line and culture conditions—The human uterine leiomyoma cell line (huLM) was kindly provided by Dr. Salama Salama (Baylor College of Medicine, Houston, TX). The cells were grown as previously described in minimum essential medium (MEM) (Gibco, NY, USA) supplemented with 19% heat-inactivated fetal bovine serum (FBS) (HyClone, UT, USA) essential and non-essential amino acids (Gibco), MEM vitamin solution (HyClone), and penicillin-streptomycin (Mediatech, Inc, VA, USA) [24]. The cells were maintained at 37°C in a humidified atmosphere of 5% CO_2 and 95% air.

• Cell proliferation and viability assay—HuLM cells express both estrogen and progesterone receptors and have been extensively used to study the effect of various antitumor drug candidates [1,6,25]. HuLM cells were seeded at a density of 2×10^3 cells/well in a 96-well plate. The cells were allowed to attach for 24 hours at 37°C. Experimental treatments were added to the cells, which were then incubated for an additional 48 hours. After 48 hours, treatments were aspirated, and 50 μL of 0.5 mg/mL MTT reagent (3-[(4,5-dimethylthiazol-2-yl]-2,5-diphenyl tetrazolium bromide) was added to each well. The plates were incubated for 3 hours. At the end of the incubation period, 100 μL of dimethyl sulfoxide (DMSO) were added to each well and the plates were allowed to shake (100 rpm) for 15 minutes. The absorbance of each well was then measured at 550 nm (having 650 nm as a reference) using a Vmax® microplate reader (Molecular Devices Corporation, CA, USA) and the data were processed using Softmax® PRO 3.0 software (Molecular Devices Corporation, CA, USA).

• Morphological observation of huLM cells—HuLM cells were seeded at 7×10^4 cells/well in a 6-well plate. The cells were allowed to grow for 48 hours at 37°C in the incubator (5% CO_2). Nanoparticles were diluted with cell culture media, and the experimental treatments were added to the cells, which were then incubated for an additional 48 hours. Thereafter, the morphological changes of huLM cells were observed with a Nikon Eclipse TS100 microscope (Japan).

Cellular uptake of coumarin-6-labelled nanoparticles

Quantitative determination of cellular uptake of nanoparticles was studied by labeling the polymeric nanoparticles with coumarin-6, a fluorescent marker, at 3.0% (w/w) theoretical load. Coumarin-6-loaded nanoparticles were prepared by the microemulsion/solvent evaporation procedure as explained above. Human leiomyoma cell lines (huLM) were cultured under the same conditions explained above, with the exception of using MEM without phenol red to avoid interference with the detection of coumarin-6.

For quantitative analysis, cells were seeded in a 24-well plate at 1×10^4 cells/well. The cells were allowed to grow to 80–90% confluency. Coumarin-6-loaded nanoparticles, diluted with HBSS, were added to the cells which were then incubated for 2 hours. After 2 hours, treatments were aspirated, and cells were rinsed three times with cold PBS. Cells were lysed overnight by adding 0.5% Triton X-100 in 0.2N sodium hydroxide solution. Aliquots of 100 μL were withdrawn for determination of the amount of coumairn-6-loaded nanoparticles taken up by the cells, which was performed by measuring the fluorescence intensity of the samples at 485 nm (excitation) and 528 nm (emission) using an FLX800 microplate reader (BioTek Instruments, Inc., VT, USA). Data acquisition was performed using Gen5™ Microplate Data Collection & Analysis software (BioTek Instruments, Inc., VT, USA). The concentration of coumarin-6 was then calculated from calibration standards prepared by serial dilution of each type of coumarin-6-loaded nanoparticles. The protein content was determined by using Pierce® BCA Protein Assay Kit according to the manufacturer's protocol (Thermo Scientific, IL, USA). Potential interference of coumarin-6 fluorescence

with the protein assay was investigated by measuring the absorbance values of standard known concentrations of coumarin-6-loaded nanoparticles diluted with protein standards, but no such interference was detected (data not shown).

For qualitative analysis, cells were seeded at 1×10^4 cells/well in chamber slides coated with fibronectin. The cells were allowed to grow to ~80% confluency. Coumarin-6-loaded PLGA nanoparticles (37.5% (w/w)), were diluted in HBSS and added to the cells, which were then incubated for an additional 2 hours. After 2 hours, treatments were aspirated, cells were rinsed three times with cold PBS, and then the cells were stained with Wheat Germ Agglutinin, Alexa Flour® 594 Conjugate (Invitrogen, CA, USA) (5 μg/mL in HBSS) for 15 minutes at 37°C. The cells were then fixed with methanol for 15 min, washed with cold PBS, and counterstained with DAPI Flouromount-G (Southern Biotech, AL, USA) for observation with a Carl Zeiss LSM510 META confocal imaging system (Carl Zeiss, Inc, Germany).

The images of the cells were recorded with following channels: blue channel (DAPI) with 364 nm excitation and 470 nm emission, green channel (for coumarin-6) with 488 nm excitation and 505–530 nm emission, and red channel (for Alexa Flour® 594) with 543 nm excitation and 560–615 nm emission.

Long-term stability of 2-ME- loaded nanoparticles

Nanoparticle dispersions were stored protected from light at 4–8°C for 12 months. The average particle size and polydispersity index were measured at different time intervals as described above.

Statistical analysis

Data collected in this study and differences among the various treatment groups in the cell viability assay were determined by analysis of variance (ANOVA) followed by Tukey's HSD multiple comparison test using JMP® 7.0 statistical software (SAS Institute Inc., NC, USA). Results with $p<0.05$ were deemed significant. The IC_{50} values (dose resulting in 50% inhibition of cell growth) were determined by non-linear regression curve fit analysis using SigmaPlot 12.0 statistical software (Systat Software, Inc., CA, USA).

Results and Discussion

Synthesis and characterization of polymer anhydrides

Poly(anhydrides) were synthesized as described in the experimental section by melt polycondensation under high vacuum [26]. To confirm the structure of the synthesized PSA and PSA-*co*-PEG, ^{1}H-NMR and DSC were utilized. ^{1}H-NMR spectra (supplementary Figure S1) show the characteristic deuterated choloroform signal at 7.26 ppm and the PSA methylene protons at 1.32, 1.65, and 2.44 ppm. Addition of PEG at 10% by weight resulted in the appearance of an additional proton signal at 3.64 ppm (indicated by the arrow in supplementary Figure S1B) corresponding to methylene protons of PEG which confirmed PEG incorporation into PSA to form the PSA-*co*-PEG. These results agreed well with ^{1}H-NMR spectra from the literature [26].

Complimentary to ^{1}H-NMR, DSC analysis was performed to verify the structures based on the melting points of the samples. Supplementary Figure S2 demonstrates the DSC thermographs of the polymers. In order to confirm the polymer/copolymer formation, DSC thermographs of the reacting monomers was also investigated (supplementary Figure S2). As shown, no glass transition temperature was observed for any of the polymers when samples were heated from 20 to 150°C. Sebacic acid and the hydroxyl-terminated

poly(ethylene glycol) (PEG, MW=8000) exhibited melting endotherms at 60.2 °C and 132.4°C, with melting enthalpy values of 779.7 and 257.9 J/g, respectively (supplementary Figure S2). Polymerization of sebacic acid monomers to produce PSA resulted in a decrease in the melting endotherm as well as the melting enthalpy. PSA had two distinct melting signals at 67.8 °C (melting enthalpy=45.3 J/g) and 62.7°C (melting enthalpy=17.1 J/g). The enthalpy was reduced in PSA because of sebacic acid polymerization which decreases the crystallinity of the latter. In order to investigate the reason for the presence of two DSC peaks for PSA, DSC cooling cycles were performed. It was found that only one exothermic crystallization peak was observed at 55.7°C (61.4 J/g) with a small shoulder at 58.2°C. The DSC peaks corresponding to PSA were attributed to different PSA polymorphs that may have been formed during the polymerization of sebacic acid. Therefore, during recrystallization of the molten PSA (cooling cycle) these polymorphs might have been arranged to form the most stable predominant polymorph which had the exothermic peak. A similar DSC pattern was observed for PSA-*co*-PEG. This polymer showed three melting signals at 57.0°C (melting enthalpy=8.2 J/g), 68.6°C (melting enthalpy=18.2 J/g), and 74.3°C (melting enthalpy=23.5 J/g). The appearance of a melting endotherm at 57.0°C implies the possibility of a partial phase separation between PEG and sebacic acid during synthesis.

HPLC method development and validation

Details concerning the HPLC method validation are described in the Supplementary Data files accompanying this manuscript.

Particle size, size distribution, zeta potential (ζ), and entrapment efficiency (EE)

2-ME-loaded nanoparticles were prepared by a microemulsion solvent evaporation method at 25°C [19]. After formulation of the nanoparticles, there was no evidence of separation or crystallization of 2-ME, as confirmed by cryo-EM, X-ray diffraction, and DSC. 2-ME incorporation into the nanoparticles was confirmed by the high entrapment efficiency (EE) values (≥ 95%).

Average particle size data, polydispersity indices (PDI), and entrapment efficiency are presented in Table 1. The average size ranged from 151 to 189 nm. The increased particle size of PLA-based nanoparticles compared to PLGA-based nanoparticles may be due to its hydrophobicity, which decreases its dispersibility by the ultrasonicator during the preparation steps. The increased hydrophobicity of PLA may also increase the viscosity and decrease the particle mobility, with a subsequent decrease in particle dispersion and increase in the particle size.

The particle size of unloaded nanoparticles made from the same polymers had comparable size measurements, implying the feasibility of entrapping 2-ME into the nanoparticles without compromising their size. It was desirable to prepare 2-ME-loaded nanoparticles with sizes below 200 nm for future *in vivo* studies.

Polydispersity index (PDI) is an indicator of particle size distribution. All nanoparticle dispersions had PDI values in the range from 0.16 to 0.26 (Table 1), indicating that the nanoparticles prepared in this work were monodisperse. Previous authors have suggested a PDI value of 0.40 as an upper limit of acceptability [27].

Typically, the ζ absolute value of 30 mV or higher would impart sufficient electrostatic repulsion between the nanoparticles, which favor their physical stability [28]. However, it has been reported that steric stabilizers (such as PVA) can produce stable nanoparticle formulations by forming a hydrophilic sheath around the particle surfaces to inhibit particle aggregation [29]. Initial assessment of the freshly prepared 2-ME-loaded nanoparticles

indicates that ζ values ranged from −11.3 to −35.5 mV. PSA-co-PEG-based nanoparticles displayed lower absolute values of ζ because of the presence of PEG chains which cover the particle surface and shield its charge. Although the ζ absolute values were less than 30 mV, the average particle size did not significantly change upon storage of the nanoformulations in the refrigerator (4–8°C) for up to twelve months (see section 3.10 below). The observed long-term stability of the nanoparticles could be attributed to presence of the stabilizer PVA.

In vitro drug release studies

The release of 2-ME from the nanoparticle formulations was measured *in vitro* over 72 hours. Because of the low water solubility of 2-ME, 1.0% Tween® 80 was added to PBS buffer (pH 7.4) to maintain sink conditions. The release profile of 2-ME from the nanoparticles shown in Figure 1 demonstrates a monophasic release pattern. The 2-ME concentration in the release medium was below the level of quantification during the first 16 hours. Thereafter, the cumulative percentage of 2-ME release over 72 hours was below 10% for all 2-ME-loaded nanoparticles. There was no burst drug release as is often observed with nanoparticles [30]. These results indicate that 2-ME is likely to remain associated with the nanoparticles, as corroborated by the high encapsulation efficiency values.

Although only a small fraction of 2-ME was released into the media over 72 hours, the 2-ME-loaded nanoparticle formulations still exerted cytotoxic effects upon huLM cells over the course of 72 hours (see sections 3.8 and 3.9 below). Examples from the literature have also shown that even when only a fraction of drug is released from nanoparticles, these nanoformulations display more antitumor activity compared to the free drug, indicating that their anticancer potency was retained even though a substantial fraction of the drug was still associated with the nanoparticles [30].

Cryo-electron microscopy (cryo-EM)

Cryo-EM allows the preservation of the native state of the samples by extremely rapid freezing of suspensions by so-called water vitrification [23]. In this process, the fast cooling rates ($> 10^5$–10^6°C/second) allows water to harden like glass, leaving the specimens embedded in a solid matrix to maintain the native conformations of biological macromolecules [31]. Cryo-EM images were collected to investigate the shape of the 2-ME-loaded nanoparticles. As shown in the representative image (Supplementary Figure S3), the nanoparticles were spherical. No 2-ME crystals were visible, which confirmed the amorphous states depicted by the XRD results. The size of the nanoparticles was measured using DigitalMicrograph software (Gatan, Inc., Pleasanton, CA). These particle size measurements agreed well with the particle size data obtained by photon correlation spectroscopy that were reported in Table 1.

Differential scanning calorimetry (DSC) studies

DSC is an established technique that has been used to characterize solid dispersions, evaluate drug-polymer interactions, and assess the degree of crystallization and polymorphism of drugs [32]. Therefore, DSC was used to study the physical state of 2-ME in the loaded nanoparticles. As described in the experimental section, 2-ME-loaded nanoparticles were freeze-dried before analysis. Appropriate freeze-drying protocols were followed in order to avoid drug crystallization during freezing and/or drying cycles. The thermographs of bulk 2-ME revealed a characteristic sharp endothermic peak at 189°C corresponding to its melting point (Figure 2). The DSC thermographs corresponding to the physical mixtures of 2-ME and unloaded nanoparticles, however, showed two distinct endothermic peaks at approximately 189°C, which corresponded to the melting point of 2-ME, and a broad peak (60–85°C) which represents an overlap of the glass transition temperature of PVA (the stabilizer) with the melting point of the polymers (in the case of

PSA and PSA-*co*-PEG) or the glass transition temperature of the polymers (in the case of PLA/PLGA). The presence of two distinctive endothermic events indicated that 2-ME, the polymers, and PVA were in a crystalline state and that an interaction did not exist between 2-ME and the polymers. In contrast, DSC profiles of the 2-ME-loaded nanoparticles revealed a single broad endotherm at 60–85°C which suggested the presence of 2-ME as a molecular dispersion in the partially crystalline polymer (Figure 2). No change was observed in the thermal plots of the 2-ME-loaded nanoparticles after 5 months of storage, thus implying good long-term stability of the nanoformulations (Figure 2).

X-ray diffraction (XRD) studies

It is well documented that nanoparticle cores have limited payload which may result in drug crystallization days to months after formulation [33]. This could lead to burst drug release immediately after nanoparticle administration. In order to incorporate a drug into nanoparticles it should be uniformly distributed in the nanoparticle matrix and be present in an amorphous state. Therefore, to study the physical state of 2-ME with the polymers and to understand the physical behavior of the nanoparticles, samples were analyzed by wide-angle X-ray diffraction (XRD), an established technique that has been used to characterize solid dispersions and evaluate the degree of crystallization and polymorphism of drugs [32,34].

To confirm the data generated by DSC, freeze-dried nanoparticle formulations were analyzed by XRD as described in the experimental section. The X-ray diffraction pattern for bulk 2-ME revealed major peaks at $2\theta = 9.6$, 13.1, 13.6, 14.6, 15.4, 22.4, 24.2, 26.1, and 27.4° (Figure 3). These peaks indicate the presence of 2-ME in crystalline form. Freeze-dried dispersions of unloaded as well as 2-ME-loaded nanoparticles displayed only the PVA-derived broad peak ($2\theta = 10–20°$). The absence of peaks distinctive to 2-ME from the diffraction pattern of the freeze-dried 2-ME-loaded nanoparticles confirms the existence of 2-ME in an amorphous state and as a molecular dispersion in the nanoparticle matrices. These data were also confirmed by cryo-EM as was described above. As with DSC, no changes in the crystallinity of the freeze-dried nanoparticles were observed after five months of storage of liquid samples at 4–8°C (Figure 3). This validates the high entrapment efficiency of 2-ME in the nanoparticles and the long-term stability of 2-ME in the nanoparticles, which will be discussed in more detail below.

Cytotoxicity studies

2-ME is a non-polar endogenous estrogen metabolite that has been reported as an apoptosis-inducing agent in various tumor cells *in vitro* [35,36]. It also has antiangiogenic activity in solid tumors. It has been shown that 2-ME exhibits *in vitro* antiproliferative and apoptotic activity against huLM cells [6]. In an attempt to determine the polymer concentration that will not adversely affect huLM cells, *in vitro* cell viability studies were carried out using blank nanoparticles (without 2-ME) with each polymer at various concentrations. Unloaded nanoparticles at polymer concentrations of 1 mg/L did not demonstrate cytotoxicity in huLM (see Figure 4). However, significant decreases in cell viability were observed upon exposure to polymer concentrations greater than 30 mg/L PLA and 2.2 mg/L PSA-co-PEG. PLGA and PSA nanoparticles did not show any significant cytotoxic effects at any concentration up to and including 30 mg/L. Fresh batches of 2-ME-loaded nanoparticles at 10% theoretical loading were prepared and displayed Z-average particle size values ranging from 164 ± 10 to 201 ± 10 nm. All PDI values were below the accepted limit of 0.40. The ζ values ranged from −17.0 ± 0.7 to −8.4 ± 0.4. The entrapment efficiency (EE) was determined and was greater than 86.4 ± 0.1%.

The effects of 2-ME (freely dissolved in 0.03% ethanol/culture medium) and 2-ME-loaded nanoparticles on cell viability over a 48-hour period are shown in Figure 4. 2-ME alone did

not display any significant cytotoxic effects on huLM cells at a concentration of 0.35 μM. On the other hand, 2-ME-loaded PLA and PLGA nanoparticles significantly ($p<0.05$) reduced cell viability at this same concentration. Decreased cell viability was also observed for PSA nanoparticles, but this effect was not statistically significant. The reduced cell viability upon exposure to the PSA-*co*-PEG nanoparticles was similar to the effect of the unloaded nanoparticles prepared from this particular polymer.

This increased cytotoxic effect might be due to internalization of the nanoparticles into the cells with subsequent 2-ME release in a sustained/controlled manner as implied in the *in vitro* release experiments. It might be also due to surface disruption of the huLM fibroblasts by the 2-ME-loaded nanoparticles. Future experiments are proposed to understand the mechanism by which these 2-ME-loaded nanoparticles exerted cell death.

Even though only a small fraction of 2-ME was released from the nanoparticles, the cytotoxicity of 2-ME-loaded nanoparticles was not diminished. Instead, the PLA and PLGA nanoparticle formulations had a more significant effect on the huLM cells compared to free 2-ME. These results confirmed the advantages of using polymeric nanoparticles as delivery vehicles for 2-ME to potentiate cytotoxic activity against huLM cells.

Morphological changes to leiomyoma cells

In cell culture medium, huLM cells produce an extracellular collagen matrix [6] and display fibroblast-like morphology [1]. For qualitative determination of the cytotoxic effect of 2-ME (freely dissolved in ≤ 0.03% ethanol/cell culture medium) and 2-ME-loaded nanoparticles, morphological changes of huLM cells were observed microscopically after the cells were allowed to grow for 48 hours in supplemented growth medium. The medium was then aspirated and replaced by treatments as explained in the experimental section. The morphologic features of huLM cells incubated with these treatments are shown in Figure 5. As shown in Figure 5B, The huLM cells displayed fibroblast-like morphology in supplemented growth medium (containing ≤ 0.03% ethanol). Addition of 1.5 μM of 2-ME (freely dissolved in ethanol/culture medium) inhibited the cell growth, discontinued the fibrous-like structure, and resulted in cell death which caused some cells to float (Figure 5C, arrows). When the cells were treated with 10 μM of free 2-ME, these changes became more significant (Figure 5D). On the other hand, huLM cells treated with 2-ME-loaded nanoparticles at 10 μM produced significant cell death with complete loss of cell integrity (Figures 5E–5H).

Long-term stability of 2-ME-loaded nanoparticles

To test the long-term physical stability of 2-ME-loaded nanoparticles, the particle size of the dispersions was measured for fresh samples and after storage for both 5 and 12 months at 4–8°C and protected from light. The particle size of the 2-ME-loaded nanoparticles did not change significantly ($p>0.05$) after storage when compared to the freshly prepared samples (Supplementary Figure S4). After 12 months, the average size of the nanoparticles increased from 184 to 200 nm, from 159 to 174 nm, from 150 to 162 nm, and from 160 to 173 nm for 2-ME-loaded nanoparticles made from PLA, PLGA, PSA, and PSA-*co*-PEG, respectively. The polydispersity index at different time points remained below 0.4 for all dispersions. These results reflected good long-term stability of the nanoparticles. This was further confirmed by the absence of visible phase separation, and the continued lack of the distinctive 2-ME endothermic peak or crystalline pattern when freeze-dried 2-ME-loaded nanoparticles were analyzed after 5 months by DSC and XRD, respectively (Figures 2 & 3).

To examine the possibility of drug expulsion from the nanoparticles during storage, dispersions were analyzed for entrapment efficiency using HPLC. The percentage of 2-ME

that remained entrapped in the nanoparticles after 12 months was > 90%, which further confirms the long-term stability of nanoformulations.

Cellular uptake of coumarin-6-loaded nanoparticles

To check the potential for these nanoparticles to be taken up by huLM cells, nanoparticles were labeled with coumarin-6, and the cell uptake was determined qualitatively by using confocal microscopy and quantitatively by measuring the percent of coumarin-6-loaded nanoparticles taken up relative to the amount of cellular protein.

Coumarin-6-loaded nanoparticles were prepared by the same emulsification/solvent evaporation method and the cellular uptake was tested *in vitro*. For quantitative determination of uptake, cells were treated for 2 hours with the coumarin-6-loaded nanoparticles diluted in HBSS. Cells were then washed and lysed overnight by adding 0.5% Triton X-100 in 0.2 N sodium hydroxide solution for determination of the fluorescence as well as the protein content.

Figure 6 demonstrates the cell uptake of coumarin-6-loaded nanoparticles composed of different polymers. As shown, the order of cellular uptake for coumarin-6-loaded nanoparticles was PSA-*co*-PEG ≈ PSA > PLA ≈ PLGA. These results indicate that polyanhydride-based nanoparticles were taken up by the cells to a greater extent than the polyester-based nanoparticles. These findings are consistent with the observed changes in morphology (Figure 5). Future studies will lead to additional understanding regarding the mechanisms of nanoparticle uptake by the huLM cells, and future *in vivo* pharmacokinetic and nanoparticle distribution studies will also be needed.

Labeling nanoparticles with coumarin-6 enables confocal microscopic imaging for qualitative determination of huLM cell uptake. In these studies, huLM cells were allowed to grow on chamber slides coated with fibronectin as described in the experimental section. Cells were treated with coumarin-6-loaded PLGA nanoparticles (at 37.5% (w/w) theoretical loading) diluted in HBSS. Confocal microscopic images were taken and compared to cells treated with HBSS (as a negative control). Figure 7A shows the internalization of coumarin-6-loaded nanoparticles into the cytoplasm of the cells after 2 hours of incubation at 37°C. The fluorescent nanoparticles (green) crossed the cell membrane (red) and were distributed in the cytoplasm near the nuclei (blue) (Figure 7A). In contrast, under similar conditions, the huLM cells treated with HBSS alone did not show similar green fluorescence signals (Figure 7B).

Conclusions

Uterine leiomyomas are the leading indication for hysterectomy, with more than 200,000 cases per year in the United State alone [37,38]. Although hysterectomy is the current treatment option, many women seek an alternative because they desire future childbearing or wish to retain their uteri even if they have completed childbearing. Herein, we propose a novel therapeutic approach using 2-ME to address the clinical condition having the biggest impact on a woman’s reproductive system. 2-ME, an endogenous estrogen metabolite formed by the sequential action of CYP450s and catechol-O-methyltransferase (COMT), has been demonstrated as a potent antiproliferative, proapoptotic, antiangiogenic, and collagen synthesis inhibitor in human leiomyomas cells (huLM) [6,39]. Despite its effect on uterine leiomyomas, 2-ME delivery to the tumors remains a challenge because of its poor aqueous solubility and low bioavailability. In order to overcome this challenge, the objective of the present investigation was to prepare 2-ME-loaded nanoparticles and use these platforms as potential antitumor therapy.

For the first time, polymeric nanoparticles prepared from biocompatible, biodegradable, and FDA-approved materials were successfully synthesized as platforms for 2-methoxyestradiol treatment of uterine fibroids. The 2-ME-loaded nanoparticles were below 200 nm in size with good long-term stability, controlled-release properties, and displayed greater cytotoxicity to huLM cells than free 2-ME. Cellular uptake of fluorescently-labeled nanoparticles showed enhanced internalization in the cytoplasm near the nuclei, which confirms the ability of these delivery systems to cross the cell membrane. Although PSA-*co*-PEG has advantages concerning transport in vaginal mucosa [40], high concentrations of unloaded nanoparticles prepared from the PSA-*co*-PEG polymer synthesized in this work displayed some toxic effects. Therefore, among the types investigated in this study, PLGA nanoparticles appear to be the most promising, as the 2-ME-loaded PLGA nanoparticles had a significant effect upon huLM cell viability, and no toxicity was observed for the unloaded nanoparticles. It may be advantageous in the future to investigate the performance of PEGylated PLGA nanoparticles in terms of both 2-ME delivery and mucosal penetration.

Future perspectives

Information derived in this report will allow investigators to explore future *in vivo* models for treatment of uterine leiomyoma. Although asymptomatic in about half of the cases, uterine leiomyomas are the most common solid pelvic tumors in women, with an estimated cumulative incidence of up to 70–80% of women by age 50 [41]. Considering that leiomyomas represent a leading indication for hysterectomy [42], this study promotes the development of an alternative medical treatment modality. As current medical treatment alternatives fail to meet expectations, it is necessary to design new and safer approaches.

Supplementary Material

Refer to Web version on PubMed Central for supplementary material.

Acknowledgments

The authors would like to thank Dr. Adriana Paulucci-Holthauzen, Dr. Gracie Vargas, and Dr. Kert Edward (Center for Biomedical Engineering, University of Texas Medical Branch) for their assistance with confocal imaging. We thank Dr. Mark White and Dr. Michael Sherman (Sealy Center for Structural Biology & Molecular Biophysics, University of Texas Medical Branch) for their assistance with X-ray diffraction and cryo-electron microscopy, respectively. We thank Dr. Salama Salama (Baylor College of medicine, Houston, Texas) for providing uterine leiomyoma cells (huLM) and Dr. Richard Hodge of UTMB's Synthetic Organic Chemistry Core Laboratory for assistance with the polymer synthesis. Funding from UTMB's Department of Obstetrics & Gynecology/Biomedical Engineering Collaborative Grant is gratefully acknowledged. Dr. Rytting is supported by a research career development award (K12HD052023: Building Interdisciplinary Research Careers in Women's Health Program, BIRCWH) from the National Institute of Allergy and Infectious Diseases (NIAID), the Eunice Kennedy Shriver National Institute of Child Health and Human Development (NICHD), and the Office of the Director (OD), National Institutes of Health. The content is solely the responsibility of the authors and does not necessarily represent the official views of the NIAID, NICHD, OD, or the National Institutes of Health.

KEY TERMS

uterine leiomyoma (fibroids)	benign solid tumors that cause heavy menstrual bleeding and affect a woman's reproductive potential
2-methoxyestradiol (2-ME)	an apoptosis-inducing medication under evaluation for treatment of uterine leiomyoma (fibroids)
hysterectomy	removal of the uterus by surgery
polymeric nanoparticles	particles with dimensions 1–1000 nm prepared with biodegradable polymers

drug release	the rate of escape of drug molecules from the nanocarrier matrix

References

Papers of special note have been highlighted as:

* of interest

** of considerable interest

1. Zhang D, Al-Hendy M, Richard-Davis G, Montgomery-Rice V, Rajaratnam V, Al-Hendy A. Antiproliferative and proapoptotic effects of epigallocatechin gallate on human leiomyoma cells. Fertil Steril. 2010; 94(5):1887–1893. [PubMed: 19819432]
2*. Stewart EA. Uterine fibroids. Lancet. 2001; 357(9252):293–298. Uterine leiomyoma results in heavy bleeding during menstruation for longer periods of times. Hystrectomy is considered one of the treatment options. [PubMed: 11214143]
3. Al-Hendy A, Salama SA. Catechol-O-methyltransferase polymorphism is associated with increased uterine leiomyoma risk in different ethnic groups. J Soc Gynecol Investig. 2006; 13(2):136–144.
4. Othman EE, Al-Hendy A. Molecular genetics and racial disparities of uterine leiomyomas. Best Pract Res Clin Obstet Gynaecol. 2008; 22(4):589–601. [PubMed: 18373954]
5. Martel KM, Ko AC, Christman GM, Stribley JM. Apoptosis in human uterine leiomyomas. Semin Reprod Med. 2004; 22(2):91–103. [PubMed: 15164304]
6. Salama SA, Nasr AB, Dubey RK, Al-Hendy A. Estrogen metabolite 2-methoxyestradiol induces apoptosis and inhibits cell proliferation and collagen production in rat and human leiomyoma cells: a potential medicinal treatment for uterine fibroids. J Soc Gynecol Investig. 2006; 13(8):542–550. 2-methoxyestradiol induces human and rat leiomyoma cell death in a concentratuion dependent manner by inhibition of collagen synthesis and interference with the G2/M cell cycle.
7. Matsuo H, Kurachi O, Shimomura Y, Samoto T, Maruo T. Molecular bases for the actions of ovarian sex steroids in the regulation of proliferation and apoptosis of human uterine leiomyoma. Oncology. 1999; 57 (Suppl 2):49–58. [PubMed: 10545803]
8. Stewart EA, Friedman AJ, Peck K, Nowak RA. Relative overexpression of collagen type I and collagen type III messenger ribonucleic acids by uterine leiomyomas during the proliferative phase of the menstrual cycle. J Clin Endocrinol Metab. 1994; 79(3):900–906. [PubMed: 8077380]
9. Barchiesi F, Jackson EK, Fingerle J, Gillespie DG, Odermatt B, Dubey RK. 2-Methoxyestradiol, an estradiol metabolite, inhibits neointima formation and smooth muscle cell growth via double blockade of the cell cycle. Circ Res. 2006; 99(3):266–274. [PubMed: 16794187]
10**. Dahut WL, Lakhani NJ, Gulley JL, et al. Phase I clinical trial of oral 2-methoxyestradiol, an antiangiogenic and apoptotic agent, in patients with solid tumors. Cancer Biol Ther. 2006; 5(1): 22–27. Clinical trial demonstrating the poor bioavailability of 2-methoxyestradiol. [PubMed: 16357512]
11*. Soppimath KS, Aminabhavi TM, Kulkarni AR, Rudzinski WE. Biodegradable polymeric nanoparticles as drug delivery devices. J Control Release. 2001; 70(1–2):1–20. Application of nanoparticulate systems for drug delivery: procedures for preparation and characteriztion. [PubMed: 11166403]
12. Bennewitz MF, Saltzman WM. Nanotechnology for delivery of drugs to the brain for epilepsy. Neurotherapeutics. 2009; 6(2):323–336. [PubMed: 19332327]
13. Kreuter J. Drug targeting with nanoparticles. Eur J Drug Metab Pharmacokinet. 1994; 19(3):253–256. [PubMed: 7867668]
14. Rahman Z, Zidan AS, Habib MJ, Khan MA. Understanding the quality of protein loaded PLGA nanoparticles variability by Plackett-Burman design. Int J Pharm. 2010; 389(1–2):186–194. [PubMed: 20038446]

15. Song X, Zhao Y, Wu W, et al. PLGA nanoparticles simultaneously loaded with vincristine sulfate and verapamil hydrochloride: systematic study of particle size and drug entrapment efficiency. Int J Pharm. 2008; 350(1–2):320–329. [PubMed: 17913411]

16. Zou W, Liu C, Chen Z, Zhang N. Studies on bioadhesive PLGA nanoparticles: A promising gene delivery system for efficient gene therapy to lung cancer. Int J Pharm. 2009; 370(1–2):187–195. [PubMed: 19073241]

17. Parajó Y, d'Angelo I, Horváth A, et al. PLGA:poloxamer blend micro- and nanoparticles as controlled release systems for synthetic proangiogenic factors. Eur J Pharm Sci. 2010; 41(5):644–649. [PubMed: 20869438]

18. Chan JM, Zhang L, Yuet KP, et al. PLGA-lecithin-PEG core-shell nanoparticles for controlled drug delivery. Biomaterials. 2009; 30(8):1627–1634. [PubMed: 19111339]

19. Jain RA. The manufacturing techniques of various drug loaded biodegradable poly(lactide-co-glycolide) (PLGA) devices. Biomaterials. 2000; 21(23):2475–2490. [PubMed: 11055295]

20. Campolongo MJ, Luo D. Drug delivery: Old polymer learns new tracts. Nat Mater. 2009; 8(6): 447–448. [PubMed: 19458640]

21*. Fiegel J, Fu J, Hanes J. Poly(ether-anhydride) dry powder aerosols for sustained drug delivery in the lungs. J Control Release. 2004; 96(3):411–423. Describes the synthesis of biodegradable polymers effective for drug delivery. [PubMed: 15120898]

22. Fu J, Fiegel J, Krauland E, Hanes J. New polymeric carriers for controlled drug delivery following inhalation or injection. Biomaterials. 2002; 23(22):4425–4433. [PubMed: 12219833]

23. Sherman MB, Weaver SC. Structure of the Recombinant Alphavirus Western Equine Encephalitis Virus Revealed by Cryoelectron Microscopy. J Virol. 2010; 84(19):9775–9782. [PubMed: 20631130]

24. Carney SA, Tahara H, Swartz CD, et al. Immortalization of human uterine leiomyoma and myometrial cell lines after induction of telomerase activity: molecular and phenotypic characteristics. Lab Invest. 2002; 82(6):719–728. [PubMed: 12065682]

25. Salama SA, Kamel M, Christman G, Wang HQ, Fouad HM, Al-Hendy A. Gene therapy of uterine leiomyoma: adenovirus-mediated herpes simplex virus thymidine kinase/ganciclovir treatment inhibits growth of human and rat leiomyoma cells in vitro and in a nude mouse model. Gynecol Obstet Invest. 2007; 63(2):61–70. [PubMed: 16954695]

26. Fu J, Fiegel J, Hanes J. Synthesis and characterization of PEG-based ether-anhydride terpolymers: Novel polymers for controlled drug delivery. Macromolecules. 2004; 37:7174–7180.

27. Dong X, Mattingly CA, Tseng M, Cho M, Adams VR, Mumper RJ. Development of new lipid-based paclitaxel nanoparticles using sequential simplex optimization. Eur J Pharm Biopharm. 2009; 72(1):9–17. [PubMed: 19111929]

28. Chan JM, Valencia PM, Zhang L, Langer R, Farokhzad OC. Polymeric nanoparticles for drug delivery. Methods Mol Biol. 2010; 624:163–175. [PubMed: 20217595]

29. Zambaux MF, Bonneaux F, Gref R, et al. Influence of experimental parameters on the characteristics of poly(lactic acid) nanoparticles prepared by a double emulsion method. J Control Release. 1998; 50(1–3):31–40. [PubMed: 9685870]

30**. Wong HL, Bendayan R, Rauth AM, Li Y, Wu XY. Chemotherapy with anticancer drugs encapsulated in solid lipid nanoparticles. Advanced drug delivery reviews. 2007; 59(6):491–504. The release profile of anticancer drugs (e.g. doxrubicin) is characterized by initial burst followed by release in sustained or controlled fasion. Although the drug release was incomplete, it possessed greater anticancer effects compared to free drug. [PubMed: 17532091]

31. Lapault J, Booy FP, Dubochet J. Electron microscopy of frozen biologcal suspensions. Journal of Microscopy. 1983; 129:89–102. [PubMed: 6186816]

32. Bunjes H, Unruh T. Characterization of lipid nanoparticles by differential scanning calorimetry, X-ray and neutron scattering. Advanced drug delivery reviews. 2007; 59(6):379–402. [PubMed: 17658653]

33. Müller RH, Radtke M, Wissing SA. Nanostructured lipid matrices for improved microencapsulation of drugs. Int J Pharm. 2002; 242(1–2):121–128. [PubMed: 12176234]

34. Jores K, Mehnert W, Mäder K. Physicochemical investigations on solid lipid nanoparticles and on oil-loaded solid lipid nanoparticles: a nuclear magnetic resonance and electron spin resonance study. Pharm Res. 2003; 20(8):1274–1283. [PubMed: 12948026]

35*. Mabjeesh NJ, Escuin D, LaVallee TM, et al. 2ME2 inhibits tumor growth and angiogenesis by disrupting microtubules and dysregulating HIF. Cancer Cell. 2003; 3(4):363–375. 2-methoxyestradiol is reported as an antiangiogenic medication that inhibits the growth of breast cancer cells. [PubMed: 12726862]

36. Ricker JL, Chen Z, Yang XP, Pribluda VS, Swartz GM, Van Waes C. 2-methoxyestradiol inhibits hypoxia-inducible factor 1alpha, tumor growth, and angiogenesis and augments paclitaxel efficacy in head and neck squamous cell carcinoma. Clin Cancer Res. 2004; 10(24):8665–8673. [PubMed: 15623651]

37. Cramer SF, Patel A. The frequency of uterine leiomyomas. Am J Clin Pathol. 1990; 94(4):435–438. [PubMed: 2220671]

38. Buttram VC, Reiter RC. Uterine leiomyomata: etiology, symptomatology, and management. Fertil Steril. 1981; 36(4):433–445. [PubMed: 7026295]

39. Salama SA, Kamel MW, Botting S, et al. Catechol-o-methyltransferase expression and 2-methoxyestradiol affect microtubule dynamics and modify steroid receptor signaling in leiomyoma cells. PLoS One. 2009; 4(10):e7356. [PubMed: 19809499]

40. Tang BC, Dawson M, Lai SK, et al. Biodegradable polymer nanoparticles that rapidly penetrate the human mucus barrier. Proc Nat Acad Sci. 2009; 106(46):19268–19273. [PubMed: 19901335]

41. Payson M, Leppert P, Segars J. Epidemiology of myomas. Obstet Gynecol Clin North Am. 2006; 33(1):1–11. [PubMed: 16504803]

42. Garry R, Fountain J, Brown J, et al. EVALUATE hysterectomy trial: a multicentre randomised trial comparing abdominal, vaginal and laparoscopic methods of hysterectomy. Health Technol Assess. 2004; 8(26):1–154. [PubMed: 15215018]

Executive summary

Introduction

- Nanoparticles encapsulating 2-methoxyestradiol (2-ME) may represent an important non-surgical, fertility-preserving alternative for the treatment of uterine leiomyoma (fibroids).

Result & Discussion

- Polyanhydride and polylactide polymers can encapsulate 2-ME in spherical, homogenous, and stable nanoparticles with diameters smaller than 200 nm and high encapsulation efficiency.
- 2-ME is released from nanoparticles in a controlled fashion with no burst release.
- Nanoencapsulation of 2-ME was confirmed by differential scanning calorimetry and X-ray diffraction.
- Unloaded polymeric nanoparticles were not cytotoxic to huLM cells at concentrations of 1 mg/L.
- 2-ME-loaded nanoparticles disrupted cellular integrity and induced cytotoxicity in huLM cells to a greater extent than free 2-ME, as evidenced by morphological observations and MTT assay.
- Uptake of fluorescent nanoparticles by confocal imaging demonstrates their ability to cross the cell membrane and reach the nuclei.

Conclusion

- Polymeric nanoparticles as efficient gynecological delivery systems represent an important therapeutic development for women seeking alternatives to hysterectomy.

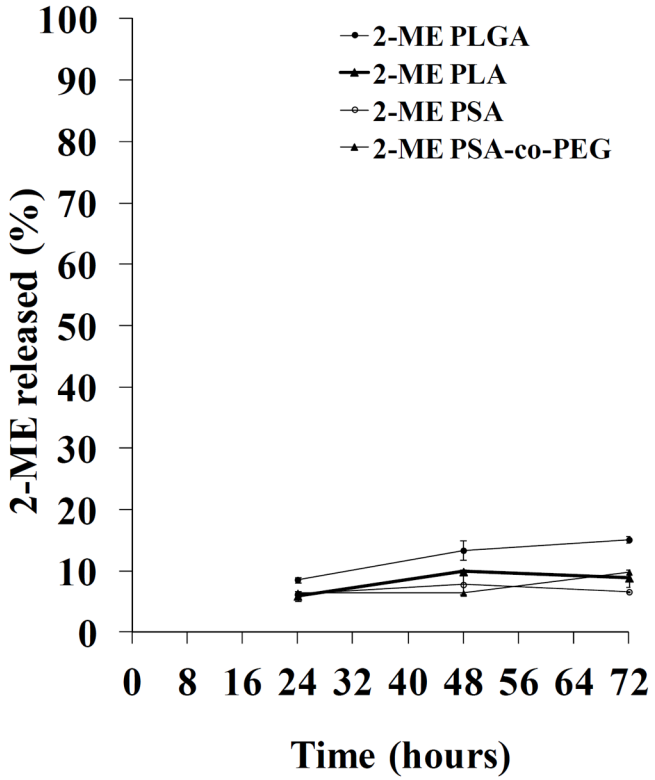

Figure 1. ***In vitro*** **release of 2-ME-loaded nanoparticles at 37°C in PBS (pH=7.4) containing 1.0% Tween® 80 to maintain sink conditions**

Scintillation vials were prepared for each time point and shaken (50 rpm) in a hot box (37°C). At each time point, 500 μL of the nanoparticle dispersion were placed in the upper chamber of the filter assembly as explained in the Materials & Methods section. The assembly was then centrifuged at 3000 rpm for 15 minutes at 25°C to separate the released 2-ME from the nanoparticles. The filtrate was diluted with the mobile phase and injected into HPLC to determine the concentration of the released 2-ME. Experiments were carried out in triplicate, and results are expressed as mean ± standard deviation.

PBS: Phosphate Buffer Saline; 2-ME: 2-methoxyestradiol; HPLC: High Performance Liquid Chromatography.

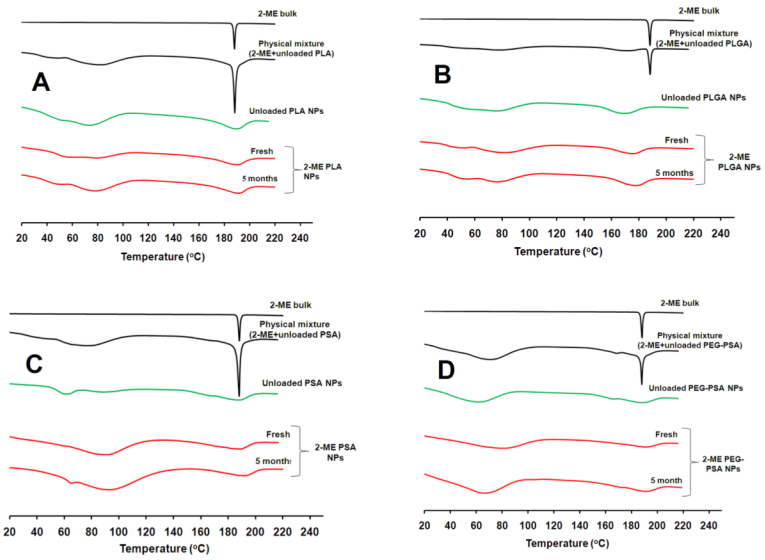

Figure 2. DSC thermographs of 2-ME-loaded nanoparticles composed of PLA (A); PLGA (B); PSA (C); and PSA-co-PEG (D)

Samples (2–3 mg), hermetically sealed in aluminum pans, were heated at a scan rate of 10°C/min from 20°C to 200°C and then allowed to cool to 10°C to observe the exothermic phase. The generated data were analyzed with Universal Analysis 2000 software. Graphs were displaced along the ordinate for better visualization.

DSC: Differential Scanning Calorimetry; PLA: polylactide; PLGA: carboxylate end group 50:50 poly(D,L-lactide-*co*-glycolide); PSA: poly(sebacic) acid; PSA-*co*-PEG: poly(sebacic acid-*co*-PEG); PEG: Polyethylene glycol.

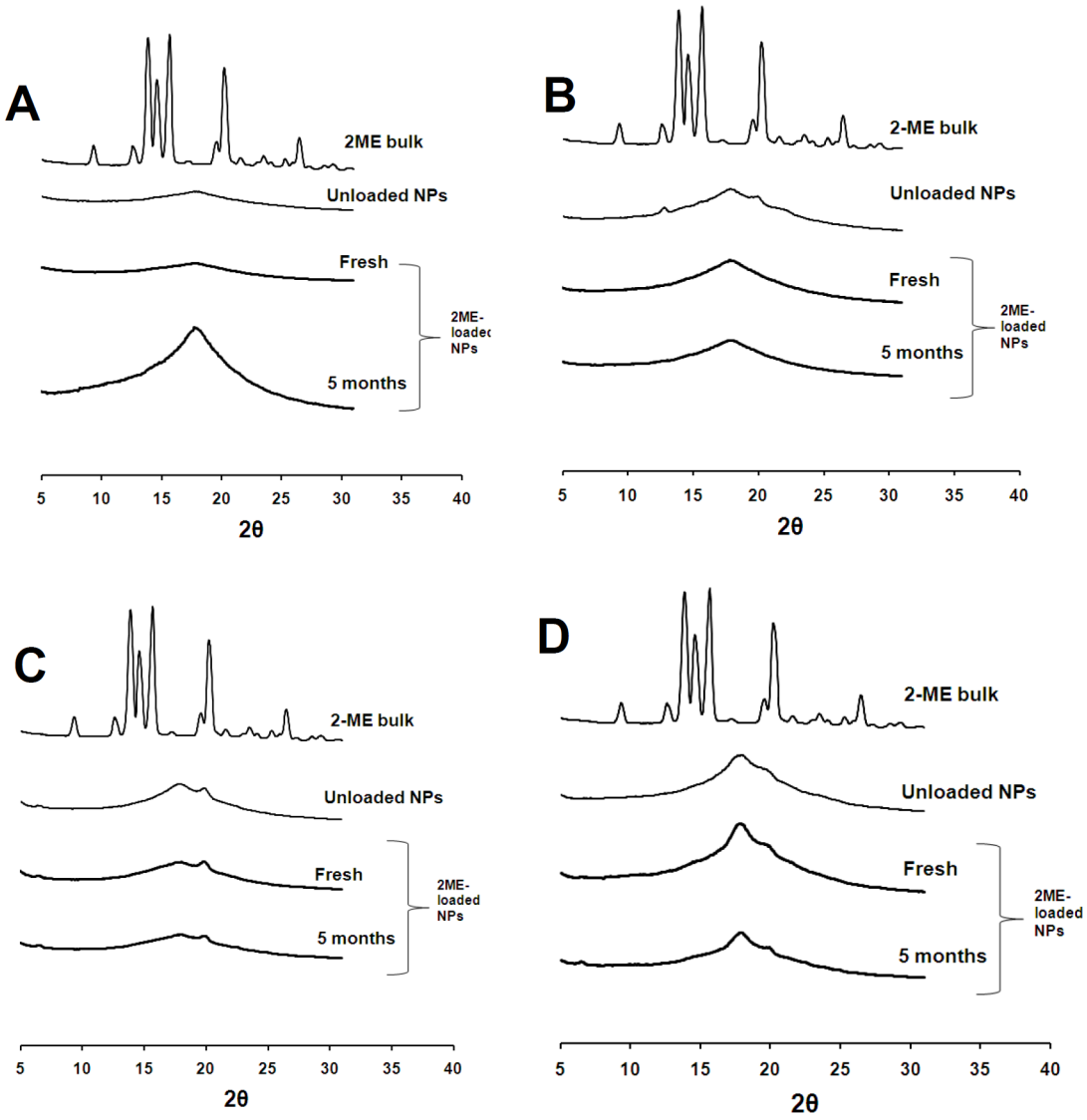

Figure 3. X-ray diffraction patterns of 2-ME, blank nanoparticles, and 2-ME-loaded nanoparticles composed of PLA (A); PLGA (B); PSA (C); and PSA-co-PEG (D)

Patterns were obtained by wide-angle X-ray scattering (2θ=5–30°, step size = 0.04). Data were recorded at an anode voltage of 40 kV and a current of 30 mA. The generated data were processed through FIT2D software to convert the image into a two-dimensional plot. Graphs were displaced along the ordinate for better visualization.

2-ME: 2-methoxyestradiol; PEG: Polyethylene glycol; PLA: polylactide; PLGA: carboxylate end group 50:50 poly(D,L-lactide-*co*-glycolide); PSA: poly(sebacic) acid; PSA-*co*-PEG: poly(sebacic acid-*co*-PEG).

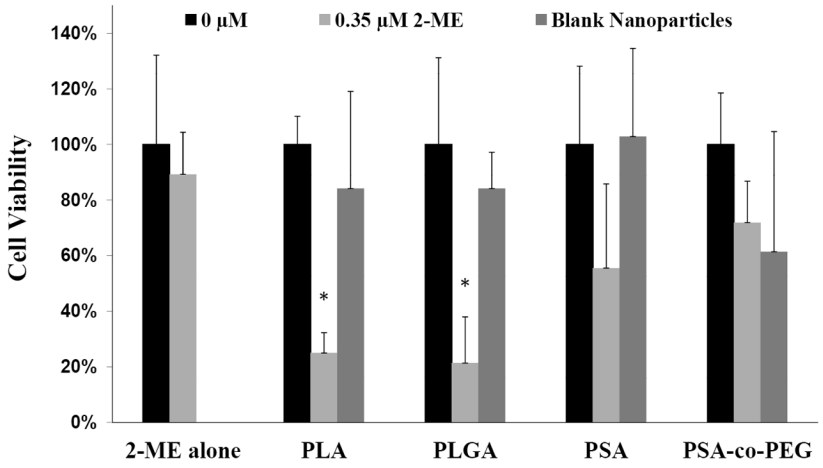

Figure 4. Cytotoxic effects on huLM cells of 0.35 μM 2-ME (freely dissolved in culture medium containing ≤ 0.03% ethanol), 2-ME-loaded nanoparticles formed of PLA, PLGA, PSA, and PSA-*co*-PEG (2-ME concentration = 0.35 μM), or blank/unloaded nanoparticles (with total polymer concentrations equal to that of the drug-loaded nanoparticles)

Cells were initially plated at a density of 2×10^3 cells/well (n=6) in 96-well plates and exposed to formulation-supplemented media for 48 hours. Cell viability was determined using the MTT colorimetric assay. Vertical bars indicate the mean cell viability as percent of control ± standard deviation. $*P < 0.05$ as compared to control (cells exposed only to cell culture medium).

2-ME: 2-methoxyestradiol; PEG: Polyethylene glycol; PLA: polylactide; PLGA: carboxylate end group 50:50 poly(D,L-lactide-*co*-glycolide); PSA: poly(sebacic) acid; PSA-*co*-PEG: poly(sebacic acid-*co*-PEG); huLM: human leiomyoma cell line; MTT: (3-[(4,5-dimethylthiazol-2-yl]-2,5-diphenyl tetrazolium bromide).

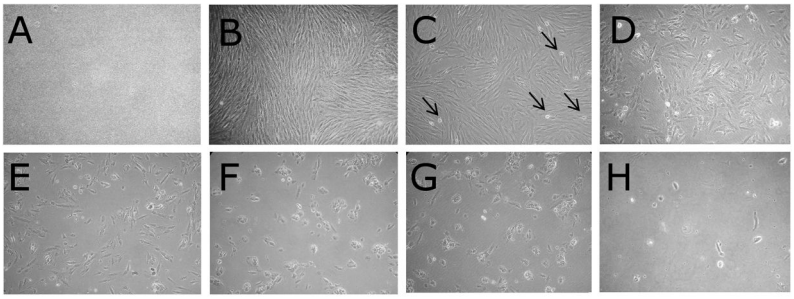

Figure 5. Morphology of huLM cells after treatment with nanoparticles and controls

(A) 0.1 % Triton-X-100 (positive control), (B) culture media with ≤ 0.03% ethanol (negative control), (C, D) 2-ME freely dissolved in ethanol/culture media at 1.5 μM and 10μM, respectively, (E,F) 2-ME-loaded PLA and PLGA nanoparticles, respectively (10 μM 2-ME), and (G,H) 2-ME-loaded PSA and PSA-*co*-PEG nanoparticles, respectively (10 μM 2-ME). HuLM cells were seeded at a density of 7×10^4 cells/well. Arrows represent dead cells. Photographs were taken by a Nikon Eclipse TS100 microscope at 10X magnification after 48 hours of treatment.

2-ME: 2-methoxyestradiol; PEG: Polyethylene glycol; PLA: polylactide; PLGA: carboxylate end group 50:50 poly(D,L-lactide-*co*-glycolide); PSA: poly(sebacic) acid; PSA-*co*-PEG: poly(sebacic acid-*co*-PEG); huLM: Human leiomyoma cell line.

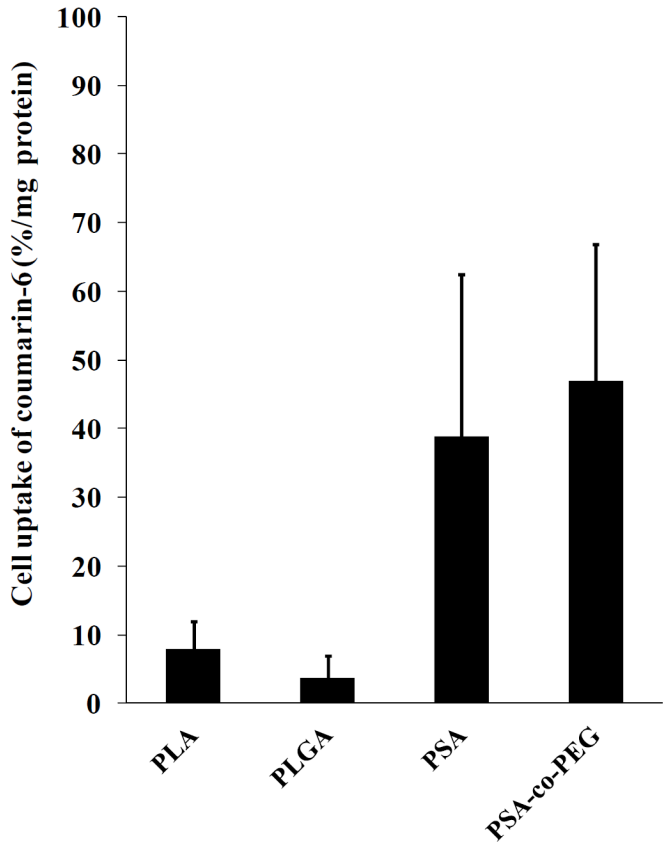

Figure 6. Quantitative cell uptake of coumarin-6-loaded nanoparticles

HuLM cells were plated at a density of 1×10^4 cells/well (6 wells/treatment) in 24-well plates and exposed to treatments diluted with HBSS for 2 hours. Cell uptake was calculated by measuring the fluorescence at 485 nm (excitation) and 528 nm (emission) after lysing the cells with 0.5% Triton X-100 in 0.2N sodium hydroxide solution. The protein content was determined by using Pierce® BCA Protein Assay Kit according to the manufacturer's protocol. Data are presented as the percentage of fluorescent nanoparticles administered to the cells per mg of total cellular protein. Vertical bars indicate the average ± standard deviation (n=6).

huLM: Human Leiomyoma Cell line; HBSS: Hank's Balanced Salt Solution.

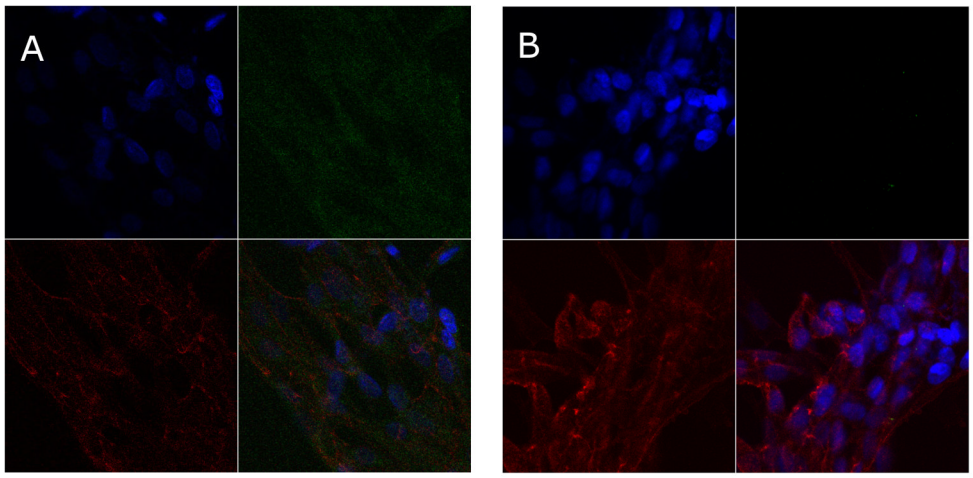

Figure 7. Confocal laser microscopy images of huLM cells after 2-hour incubation with coumarin-6-loaded PLGA nanoparticles (A) and HBSS (negative control) (B) at 37°C

Upper left are nuclei counterstained with DAPI (blue), lower left are cell membrane counterstained with Wheat Germ Agglutinin, Alexa Fluor® 594 conjugate (red), upper right are coumarin-6-loaded nanoparticles (green), and lower right is an overlaid image.

huLM: Human Leiomyoma Cell line; PLGA: carboxylate end group 50:50 poly(D,L-lactide-*co*-glycolide); HBSS: Hank's Balanced Salt Solution.

Table 1

Particle size, polydispersity index (PDI), zeta potential (ζ), and entrapment efficiency data of 2-ME-loaded nanoparticles. Results are average of triplicate measurements ± standard deviation.

Polymer*	Particle size (nm)	Polydispersity index (PDI)	Zeta potential (mV)	Entrapment efficiency (%)
PLA	189 ± 2	0.16 ± 0.01	−11.3 ± 0.2	97.7 ± 0.04
PLGA	159 ± 2	0.18 ± 0.00	−22.2 ± 0.7	95.8 ± 0.30
PSA	151 ± 7	0.26 ± 0.04	−35.5 ± 0.8	96.8 ± 0.30
PSA-*co*-PEG	161 ± 1	0.20 ± 0.03	−20.0 ± 0.6	95.8 ± 0.03

*PLA: polylactide

PLGA: carboxylate end group 50:50 poly(D,L-lactide-*co*-glycolide).

PSA: poly(sebacic) acid.

PSA-*co*-PEG: poly(sebacic acid-*co*-PEG).